J Nanostruct 11(4): 698-710, Autumn 2021

RESEARCH PAPER

Cytotoxicity and Antibacterial Activities of Coated and Non-Coated Magnetic Nanoparticles

Rania Hasan Huseen [1], Ali A. Taha [2] and Adi M. Abdul Hussien [1]*

[1] *Biotechnology Division, Applied Science Department,University of Technology, Baghdad, Iraq*

[2] *Physics Division, Applied Science Department, University of Technology, Baghdad, Iraq*

ARTICLE INFO

Article History:
Received 29 May 2021
Accepted 08 September 2021
Published 01 October 2021

Keywords:
Antibacterial activity
Cytotoxicity
Gelatin
Gum Arabic
Iron Oxide Nanoparticles

ABSTRACT

In this study, samples of iron oxide nanoparticles in magnetic form (MNPs) were produced by co-precipitation technique. Prepared MNPs was coated with gelatin or gum Arabic to decrease toxicity and enhance stability. The characteristics of coated and uncoated MNPs were investigated. Structurally, X-Ray Diffraction (XRD) indicated that the produced nanoparticles were pure and crystalline, with diameter averages of 27.21, 39.35, and 55.30 nm for MNPs, gelatin-coated MNPs, and gum Arabic-coated MNPs, respectively. Spectrophotometry, Fourier Transfer Infrared Spectrophotometer (FTIR), Energy Dispersive X-ray Spectroscopy (EDS), Zeta Potential, and Field Emission Scanning Electron Microscopic (FE-SEM) had been used for more characterization. In contrast, the bioactivity of coated and uncoated NPs was determined. The antibacterial activity of the nanoparticles was evaluated using the well diffusion method against Escherichia coli and Staphylococcus aureus. MNPs demonstrated significant and large diameters of growth were 27.5 and 30 mm against S. aureus and E. coli at 1000 µg/ml, respectively, but coated MNPs with either gelatin or gum Arabic had weak antibacterial activity against both species tested. Finally, the MTT assay was used to determine cytotoxic of coated and non coted MNPs against cancer cell line (MCF-7) and normal cells (WRL68) as a control. MCF-7 had a viability of 65.1% in the presence of 400 g/ml of prepared MNPs, whereas WRL68 had a viability of 75.03 % . on the other hand , GAM demonstrated considerable vitality of 69.9% when examined against MCF-7, while it was 80.05% against normal cell line. GAM is a good example in this regard.

How to cite this article
Huseen R H, Taha AA and Hussien A M. Cytotoxicity and Antibacterial Activities of Coated and Non-Coated Magnetic Nanoparticles. J Nanostruct, 2021; 11(4):698-710. DOI: 10.22052/JNS.2021.04.008

INTRODUCTION

Nanotechnology is a discipline that includes instruments, systems, and applications that are used in materials manufacturing on the nanoscale (1-100 nm) in order to make them lighter, quicker, stronger, more durable, and more effective [1]. It also has an influence on many sectors of life, including as pollution control, electrical and biological applications, informatics, food, and medicine [2]. Nanoparticles exhibit properties and characteristics due to their small size, chemical composition, and surface structure. The unique characteristics and physical changes of diverse nanoscale materials have led to the creation of industrial product qualities, resulting in a significant and important growth in industrial and medical applications [3]. A nanoparticle is a spherical collection of atoms or molecules with a number of atoms or molecules ranging from a one to less than million. The nanoparticles size impacts its physical behavior such electrons , conductivity , and in atoms vibrating . In addition, the mechanical characteristics of the nanoparticles have changed significantly, making them more pliable and retractable [4]. MNPs are the vast prevalent compounds found in different ecosystems, and

* *Corresponding Author Email: Ali.a.taha@uotechnology.edu.iq*

This work is licensed under the Creative Commons Attribution 4.0 International License.
To view a copy of this license, visit http://creativecommons.org/licenses/by/4.0/.

they may be found in a variety of other different chemical forms synthesized by a variety of aqueous processes (oxidation and reduction). Magnetite, hematite, akageneite , lepidocrocite, and goethite are examples of MNPs with different compositions depending on valence of iron and structure purity . MNPs (Fe_3O_4) are made up of ferric and oxygen atoms and have a particle diameter ranging from 1 to 100 nm. Nanoparticles have played a significant role in a range of applications due to their unique properties [5-8]. Moreover, MNPs surface area are larger than volume ratio, that provide good conjugation and dispersion properties in reaction media. Furthermore, MNPs has biocompatible and magnetic properties, and these features made them more attractive for different applications. They are also very stable in water under challenging circumstances such as heating and high alkalinity, making biomolecule binding comparatively straightforward [6].

Coating technology has become more widely used in manufacturing systems in recent decades to overcome the challenges in applications, as in harsh environments [9]. Despite growing interest in nanoparticles, they have a number of disadvantages, including a high rate of agglomeration, dispersion, and chemical instability. As a result, it's only useful in a few industrial and medical settings [10].

Due to its stability in strong acidic media, very low toxicity, biocompatible, and biodegradable, gum Arabic is a hydrocolloid emulsifier that widely used in industries. Gum Arabic includes monosaccharides , acids , proteins with less than 16% of moisture. Other study found that the gum Arabic contents altered according to the soil environment, tree source, and other factors that may have played a role [11].

Gelatin is a biopolymer (animal-derived protein) produced by hydrolyzing collagen protein with acids and bases. Gelatin is a transparent gel that may be found in the bones and skin of animals, especially pig and cattle. The intrinsic properties of gelatin differ depending on the kind of gelatin and the animal source [13]. High plasticity, emulsification, thickening agent, water solubility, non-toxicity, better cell adhesion, reduced cost, and the food product's tensile factor are all advantages of gelatin. Glycine (27%), proline and hydroxyproline (25%), glutamine acid (10%), alanine (9%), protein arginine (8%), and other amino acids are among the necessary proteins found in gelatin [14]. Gelatin was utilized as a covering for iron oxide nanoparticles because of its biocompatibility and biodegradability under physiological circumstances. Moreover, the

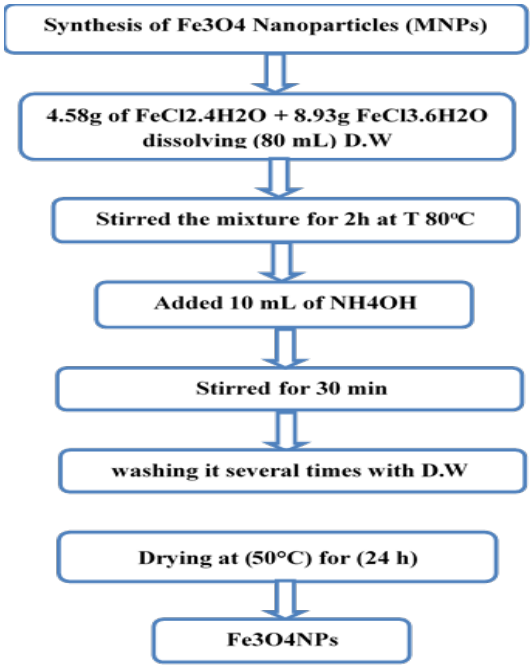

Fig. 1. Flow chart of MNPs (Fe_3O_4) synthesis.

CC BY

presence of active groups (carboxyl and amine) on the gelatin surface, as well as the charges derived by the pH, making it suitable for electrostatic adsorption and interaction with nanoparticle surfaces [15,18].

MATERIALS AND METHODS

Synthesis of Magnetic iron oxide Nanoparticles (MNPs)

The co-precipitation technique was utilized for Fe^{3+} ions and Fe^{2+}ions to manufacture magnetic Fe_3O_4 nanoparticles in the presence of ammonium hydroxide solution (NH_4OH). The step is carried out by dissolving 4.58g of $FeCl_{2.4}H_2O$ in an aqueous solution and combining it with 8.93g of $FeC_{l3.6}H_2O$. (80 mL). The solution was then heated to 80 °C while being continuously stirred. After heating the reaction solution, 10 mL of NH_4OH solution is added. Without altering the reaction conditions, the crystal growth continues for 30 minutes. The reaction solution is then purified by repeatedly rinsing it with distilled water and drying it in a 50 °C on oven [16] as show in Fig .1.

Coating of MNPs with gum Arabic (GAM)

MNPs coated by gum Arabic (GAM) was created via combining 0.5 g of Fe_3O_4 powder and 5 mg/L gum Arabic solution (50 ml). After mixing, the reaction solution was placed in a sonication bath at room temperature for 30 minutes. The

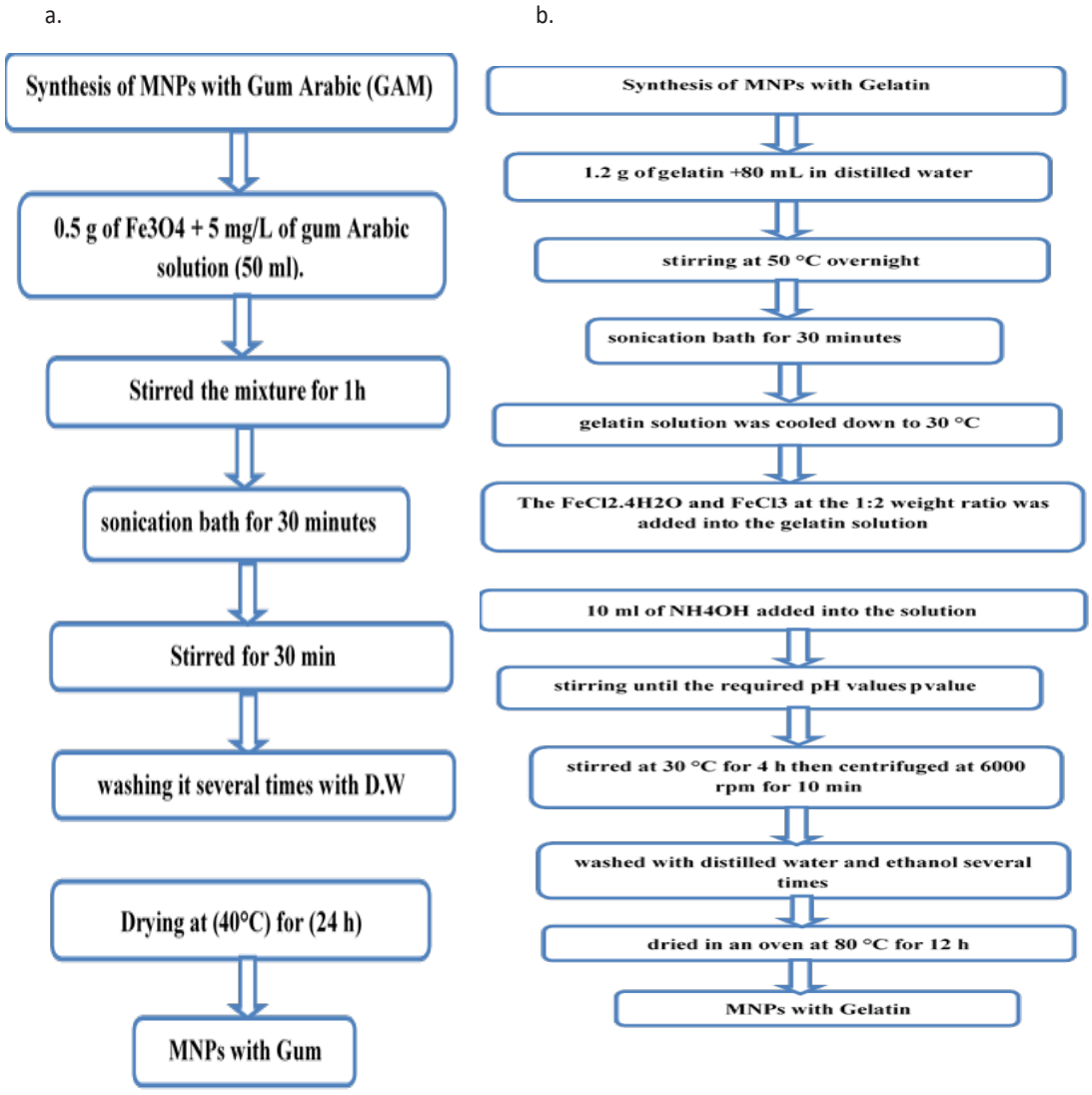

Fig. 2. The flow chart of MNPs synthesis and coated with (a) GAM, (b) GM.

CC BY

nanoparticles are then returned to the reaction solution by placing a magnet beneath the container. Finally, the resultant solution is cleaned multiple times with distilled water and dried for 24 hours in an oven at 40 °C [12]. As shown in Fig 2, a.

Surface Modification of MNPs with Gelatin (GM)

A gelatin solution was made by agitating a solution containing 1.2 gram of gelatin in 80 mL of distilled water overnight at 50°C. The obtained solution of gelatin chilled to 30 °C. The solution was then cooled to 30 °C . Thereafter, chemical reagents of $FeCl_2.4H_2O$ and $FeCl_3$ were added to the gelatin solution in a 1:2 weight ratio and agitated continuously at 30 °C for one hour to produce a brownish colloidal solution. Then, while stirring continuously, 10 mL of NH_4OH solution mixed with the solution until the pH value reached the required pH value and the resultant suspension became black. Then centrifuged at 6000 rpm for ten minutes after being agitated continuously at 30 °C for 4 hours [17], as shown in Fig 2, b.

Characterization of coated and non-coated MNPs

The crystal structure and size of the prepared coated and non-coated MNPs were determined using an X-ray diffraction (XRD-6000, Shimadzu) analysis. Chemical groups were determined using the FTIR spectroscopy (8400S, Shimadzu) in the range of 400-4000 cm^{-1}. On the other hand, field emission scanning electron microscope (FE-SEM) (Hitachi Type S-4160) had been used to determine the morphology of the produced materials, while UV-1800 spectrophotometer (Shimadzu, Kyoto, Japan). The UV-Vis was applied to determine the absorption spectra of samples.

Estimation of Antibacterial property of prepared MNPs

Well diffusion technique was used to estimate antibacterial activity of coated and non-coated MNPs . In brief , fifty microliters of bacterial suspensions of either E. coli or S. aureus (10^6 CFU/ ml) was dispersed on the sterilized Mueller-Hinton agar in Petri plates. Each well was filled with varied concentrations of MNPs, GAM and GM ranging from 250-1000 µg/ml Dimethyl sulfoxide (DMSO). The plates were incubated for 24 hours at 37 °C. DMSO was used as a control for antibacterial activity. Duplicate treatments' average inhibition zones (mm) were calculated [19].

Cytotoxicity determination of prepared MNPs

Cancer cell(MCF-7) and normal cell (WRL68) lines were cultured in RPMI/1640 medium in 96-well tissue culture plates includes 10^4 cells/ml for 48 hours at 37°C with 5% CO_2. To evaluate the toxicity, of coated and non-coated MNPs against cell lines, the cells were examined in triplicate at different concentrations of 20 - 400 µg/ml within 24 hours. Then, each well received 10 µl of MTT solution, and the plates were incubated at 37 °C for 4 hours. To determine toxicity, the medium was removed and the formazan crystals deposit was mixed with DMSO. Finally, the absorbance was measured at 570 nm using an ELISA microplate reader. The equation (1) was used to compute the cytotoxicity percentage [21].

$$\text{Cytotoxicity}(\%) = (A-B)/A \times 100 \quad (1)$$

Where: A = an absorption of the control. B = absorption of the examined sample.

RESULTS AND DISCUSSION

Characterization of prepared MNPs

X-ray diffraction (XRD) analysis

The X-ray diffraction technique is a versatile method for accurately determining various phases, crystal structure, impurities, lattice strain, and crystallite size of prepared crystalline nanomaterials. Bragg's diffraction law (2) is used to operate the x-ray diffractometer. In the present work, the samples of MNPs, GAM and GM were characterized by x-ray diffraction at room temperature with Cu-Kα radiation (λ = 1.54056 Å) in the range of $20° \leq 2\theta \leq 70°$. Fig. 3 illustrates the XRD patterns for the MNPs, GAM and GM. For this analysis, we used the card number (JCPDS Card No: 19-629). The XRD patterns of MNPs samples display diffraction peaks that were 2θ = 30.77°, 36.42°, 43.48°, 54.53°, 56.78°, and 62.28°, respectively, corresponding to the hkl planes of (220), (311), (400), (422), (511), and (440). The absence of additional peaks in the spectrum shows that the MNPs are of high purity [22]. On the other hand, the XRD patterns of GAM samples revealed diffraction peaks of 2θ = 30.05°, 36.21°, 43.65°, 54.31°, 56.08°, and 62.44° respectively, corresponding to the hkl planes of (220), (311), (400), (422), (511), and (440). Finally, the XRD patterns of GM and its diffraction peaks were 2θ = 30.93°, 36.59°, 43.37°, 54.34°, 56.28°, and 62.58° respectively, corresponding to the hkl

CC BY

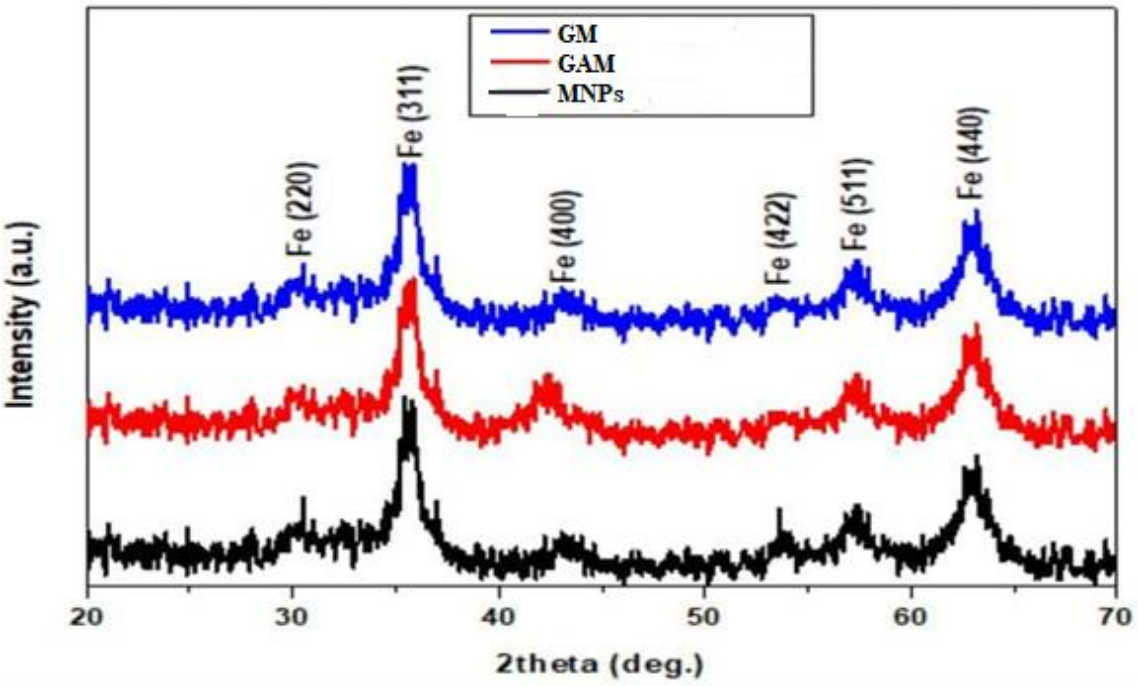

Fig. 3. XRD analysis of MNPs, GAM and GM.

planes of (220), (311), (400), (422), (511), and (440). According to the Debye Scherer's equation [23], the average crystal size was 31.27, 49.33 and 36.61 nm for MAPs, GAM and GM, respectively.

$$D = (K\lambda) / (\beta \cos\theta) \quad (2)$$

Where: k = is constant is equal to (0.94). θ = is Bragg's diffraction angle in degree. λ = is the wavelength of (Cu-Kα) radiation= 1.54 Å. β = the full-width half maximum of pattern peaks in radians.All of the diffraction peaks were found to be consonant to the diffraction peaks of the non-coated MNPs spectrum. The existence of large, high-intensity peaks also reveals the crystalline structure of the materials. Because the diffraction peaks in the spectrum are removed or displaced, the XRD data show that gelatin and gum Arabic have no influence on the crystalline nature and phase of the MNPs. This means that the NPs

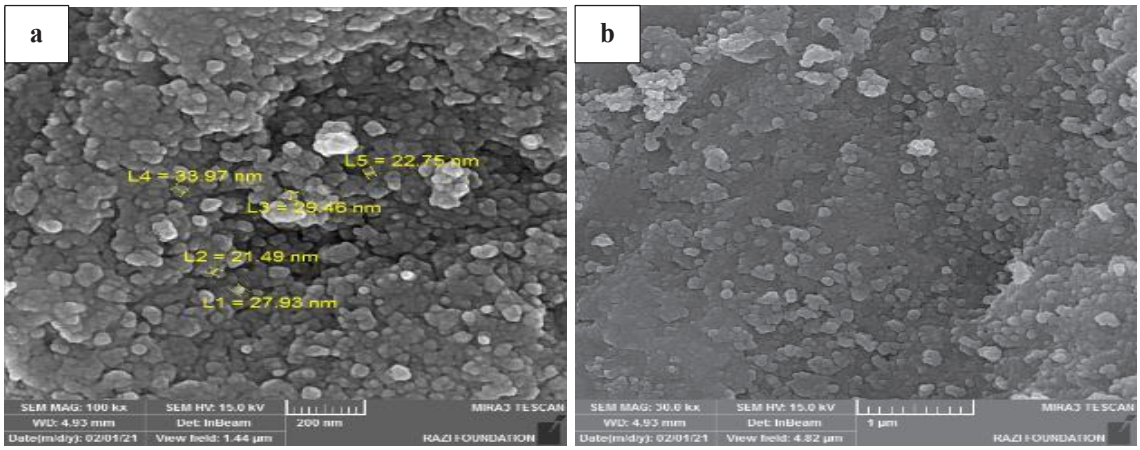

Fig. 4. FE-SEM images of MNPs with different magnifications a) at scale bar = 200 nm and b) scale bar =1 µm.

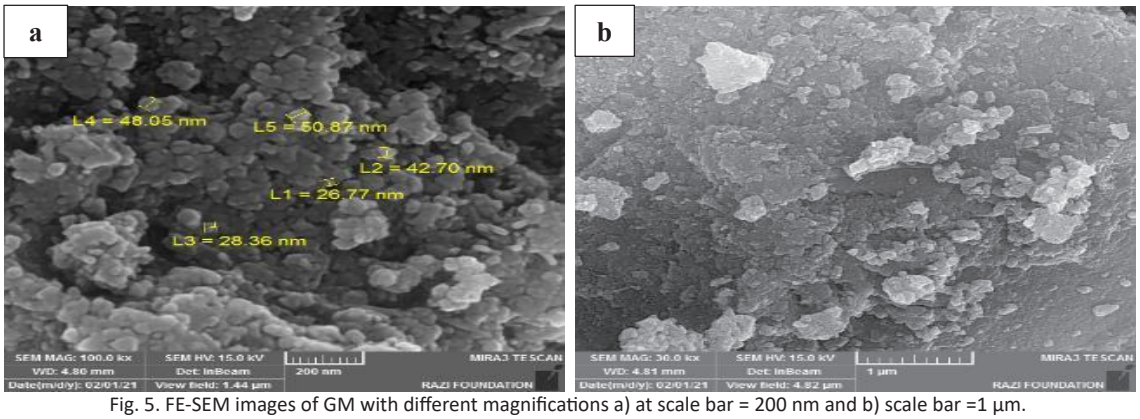

Fig. 5. FE-SEM images of GM with different magnifications a) at scale bar = 200 nm and b) scale bar =1 µm.

coating process went well. The findings are consistent with previous studies [24,25].

Field-Emission Scanning Electron Microscopy (FE-SEM)

FE-SEM is a quantitative technique that may depict morphology and particle size of a nano specimen. FE-SEM images of non-coated MNPs was illustrates in Fig. 4. The micrographs show the production of spherical MNPs of various sizes and distributions. The electrostatic contact between the layers of NPs also caused an increase in the rate of agglomeration. The diameter average of MNPs is 27.12 nm, which is similar to the crystal size determined by XRD that indicate the production of MNPs and consistent with previous study [26]. On the other hand, the FE-SEM study of GAM was shown in Fig. 5. The pictures from the FE-SEM indicate a homogenous structure with spherical forms that are closely linked. When comparing non-coated to coated MNPs, the average particle size was raised to 55.30 nm. The substantial increase in particle size is due to NPs agglomeration caused by the interaction of MNPs with the high molecular weight gum Arabic. The findings are consistent with those of a previous study [27]. Moreover, the FE-SEM analysis of the GM exhibits dense clusters of spherical forms and a limited size distribution, as shown in Fig. 5. Furthermore, as compared to naked MNPs, GM demonstrated a faster rate of particle aggregation and a larger particle size of up to 39.35 nm. This indicates the formation of MNPs covered with gelatin, and the results are similar to the results obtained Babita et al [24].

Ultraviolet-Visible Spectroscopy

The spectra of MNPs display continuous absorption along wavelengths with no significant absorption peaks. The results are identical to the

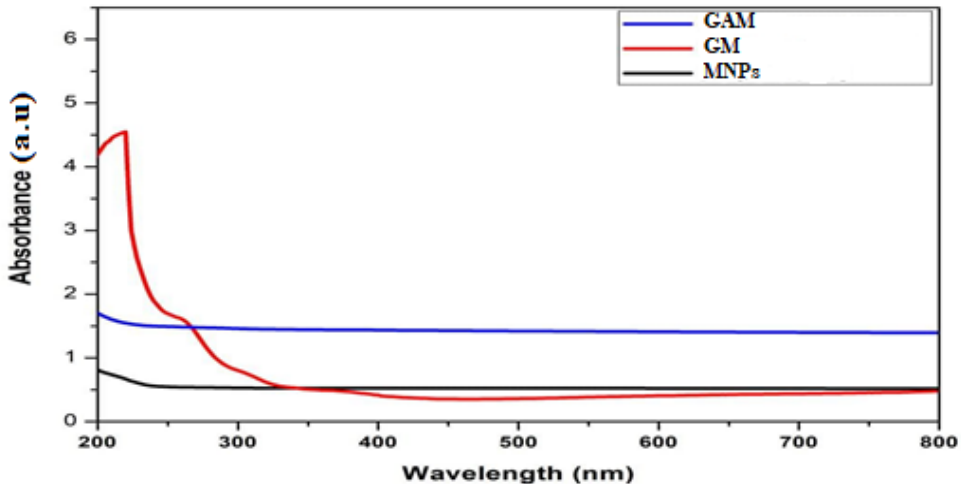

Fig. 6. Spectra of coated and non-coated MNPs.

CC BY

results introduced in Nagaraj B et al [28] and Yen P et al studies [29]. Whereas the absorption spectra of GAM exhibit a modest absorption peak at 249nm due to the presence of amino acids in gum Arabic such as aromatic amino acids [30]. Finally, the absorption spectra of GM exhibit a significant absorption peak at 217 nm due to π-π* electron transitions of peptide bonds and aromatic ring side chains. The weak absorption peak at 262 nm is caused by the n-π* electron transitions of the lateral aromatic rings. It was also discovered that the absorption peak at 217nm had a larger intensity than the absorption peak at 262nm due to the protein's higher number of peptide bonds than the aromatic rings in the gelatin composition as Fig. 6.

Fourier-Transform Infrared Spectroscopy (FTIR)

The analytical technique of FTIR spectroscopy is used to detect of chemical groups in prepared solid samples. FTIR transmission spectra of MNPs, GAM and GM in the 400-4000 cm^{-1} range. The FTIR spectra of MNPs before and after coating with gum Arabic and Gelatin presents in Fig. 7. The FTIR spectra of MNPs samples before coating, which shows the formation of peak at 3433.89 cm^{-1} related to hydroxyl group stretching vibration. This means that the water molecules have been absorbed on the surface of the prepared sample, while the hydroxyl bending vibration is responsible for the apparent absorption peak at 1647.44 cm^{-1}. Moreover, high absorption peak at 567.39 cm^{-1} is caused by the vibration of the ferrous oxygen bonds. Similar analysis observed in previous study prepared by Haiyan et al [32]. On the other hand, the GAM spectra show a broad absorption peak in region of 3500-3700 cm^{-1} caused by hydroxyl groups vibration linked with heterocyclic strictures. While the absorption peak at 2873.91 cm^{-1} is caused by the methane group (C-H) symmetric stretching vibration. The absorption maxima at 2107.35 and 1999.89 cm^{-1} are caused by CO_2 vibration. The carbonyl stretching vibration is responsible for the absorption peak at 1767.87 cm^{-1}. In addition, the peak at 1319.9 cm^{-1} is caused by the O-H bending vibration. Group of (C-O) vibration is responsible for the peak at 1252.66 cm^{-1}. High peak at 648.68 cm^{-1} is caused by the ferrous oxygen vibration. The results demonstrate the production of GAM [33]. In contrast, the FTIR spectrum of GM revealed the N-H stretching vibration of the amide groups in the gelatin structure caused a broad peak in the region 3100-3300 cm^{-1}. The C-H stretching vibration of amide is responsible for the apparent peak at 3036.75 cm^{-1}. The C=O stretching vibration of the main amide (I) and the N-H stretching vibration of the secondary amide (I) cause absorption maxima at 1632.73 and 1512.22 cm^{-1} (II). Furthermore, C-N and N-H bonding vibrations associated with the triple amide groups are attributed to the absorption peaks at 1429.56 and 1327.48 cm^{-1}. The peak at 562.72 cm^{-1} is due to the ferrous oxygen vibration. By absorbing iron ions on the amide bonds of gelatin, the FTIR measurement reveals that the coating process of iron oxide with gelatin was successful [34].

Measurements of Zeta Potential

The zeta potential value of the MNPs before coating procedure was found to be up to 10.5 mV , as shown in the Fig. 8. The attraction of the particles by the Van der Waals force causes

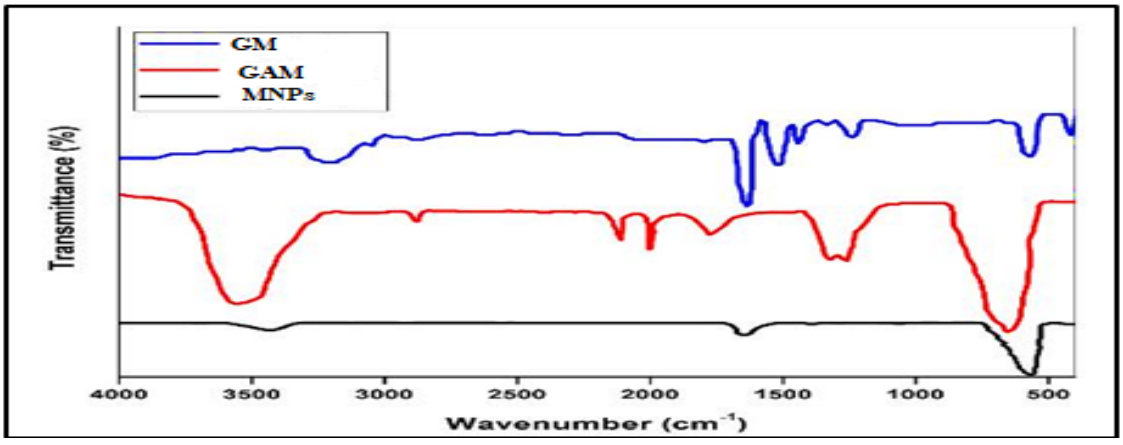

Fig. 7. FTIR spectra of coated and non-coated MNPs.

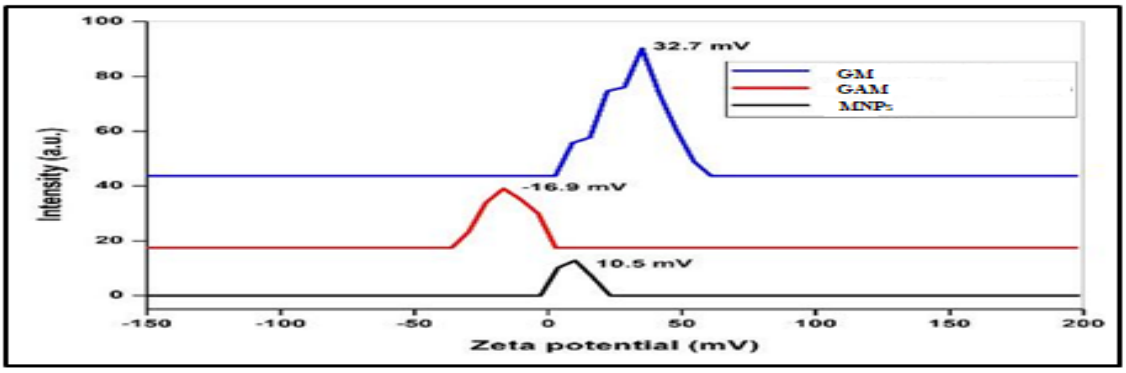

Fig. 8. Zeta potential of coated and non-coated MNPs.

the colloidal stability of the MNPs solution to diminish. Zeta potential of GAM increased to -16.9 mV. When coated MNPs was compared to naked MNPs, the zeta potential value was found to be higher. Due to the increased repulsion forces between the particles, this implies that the produced suspended solutions are stable. On the other hand, GM has zeta potential of up to 32.7 mV. The significant increase in the zeta potential value gives better physical stability to the suspended solution caused the higher electrostatic repulsion forces among the NPs . The findings support the effectiveness of the coating procedure for MNPs using gelatin and gum Arabic.

Generally, surface charge and physical stability of prepared colloidal solutions determined easily and more precisely by zeta potential analysis. When zeta potential values is greater than (+/-15) , that indicate the physical stability of the dispersed medium owing to electrostatic repulsion between nanoparticles with identical electrical charges, which increases dispersion and prevents accumulation. On the other hand , when zeta potential values is low, this implies a loss in physical stability by making the attraction forces stronger than the repulsion forces, resulting in the aggregation of NPs [35].

Energy Dispersive X-ray Spectroscopy (EDS)

EDS technique is used for determining the chemical composition of prepared samples' basic components. EDS spectra of MNPs, GAM and GM were presented in Fig. 9. The presence of a high peak for oxygen and a weak peak for iron indicates the production of the MNPs compound. Table (1) reveals that the oxygen content is 43.87 wt.% and the iron content is 50.43 wt.%. When compared to the spectrum of MNPs , the EDS

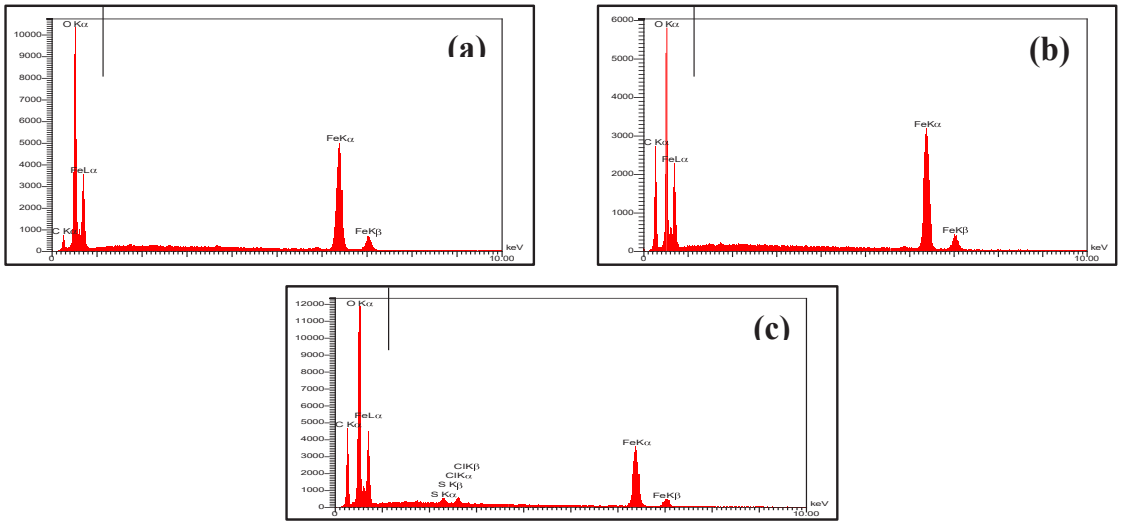

Fig. 9. EDS spectra of samples; a) MNPs, b) GAM, and c) GM.

CC BY

Table 1. The proportion of elements of prepared coated and non-coated MNPs.

Sample	C	O	Fe	S	Cl
MNPs	5.70	43.87	50.43	–	–
GAM	20.08	39.85	40.07	–	–
GM	22.33	49.18	23.53	2.40	2.56

spectra of GAM exhibits a strong peak of oxygen with a greater than carbon peak. This shows that the MNPs coating procedure with gum Arabic was successful. The oxygen content is 39.85 wt.%, the iron content is 40.07 wt.%, and the carbon content is 20.08 wt.% [12]. Due to the existence of the MNPs compound, EDS analysis of MNPs coated with gelatin reveals an oxygen content of 49.18 wt.% and an iron content of 23.53 wt.%. The gelatin component is responsible for 22.33 wt.% of the carbon. The results are identical to previous studies prepared by Saddam et al. [19].

Antibacterial Activities of coated and non-coated MNPs

Variable concentrations of MNPs before and after coating were tested against E. coli, and S. aureus as Gram-negative and Gram-positive

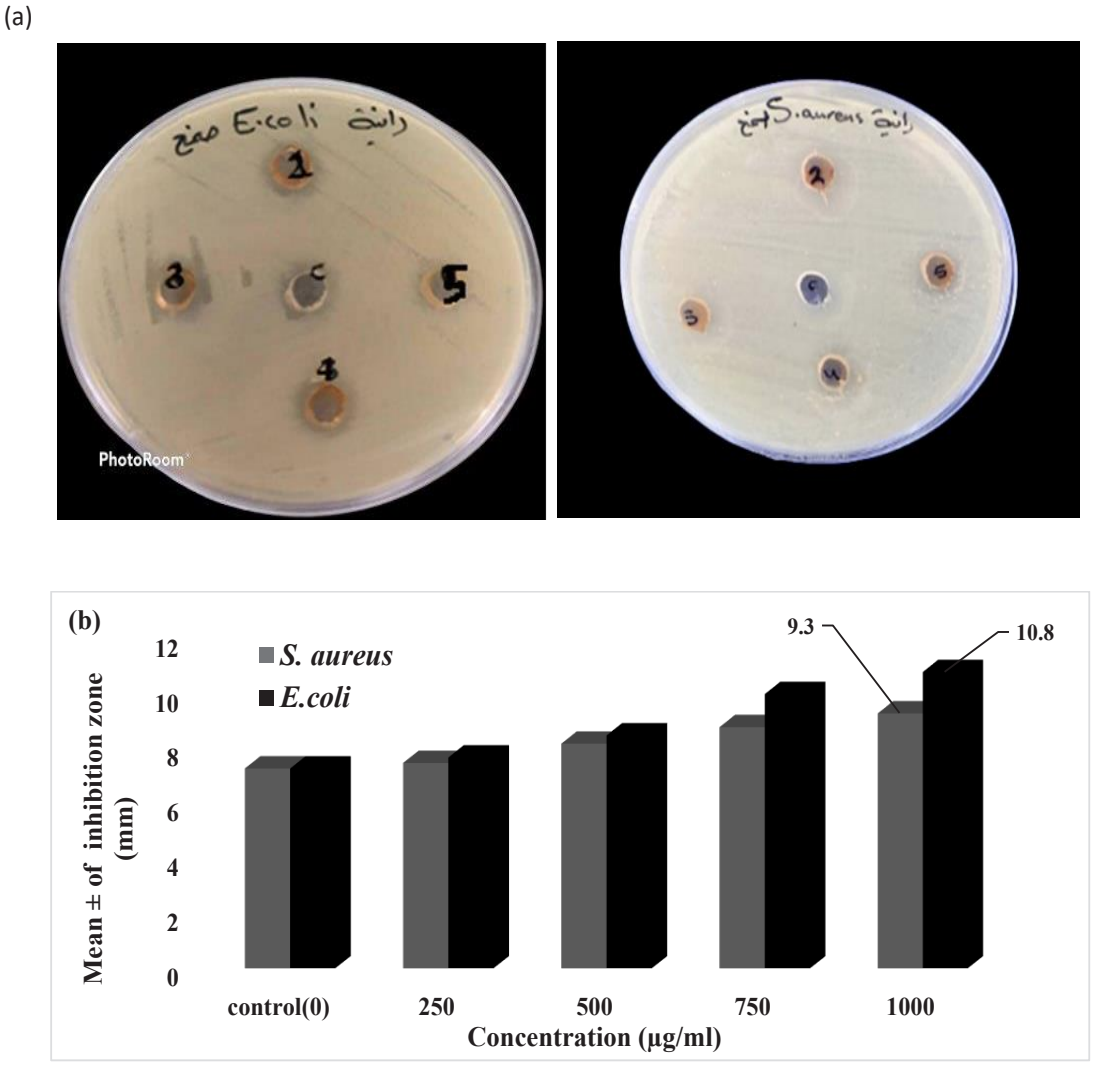

Fig. 10. Growth inhibition zone produced by MNPs against bacteria on Muller-Hinton agar (a) and statistical analyses (b). The control includes only DMSO.

CC BY

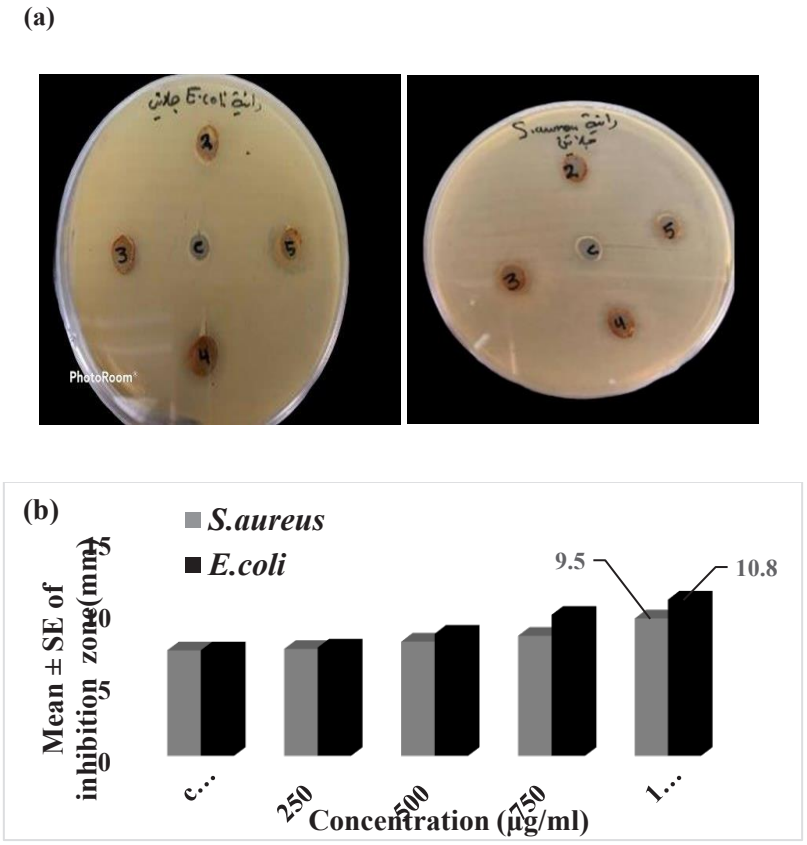

Fig. 11. Growth inhibition zone produced by GM against bacteria. on Muller-Hinton agar (a), and statistical analyses (b). The control includes only DMSO.

bacteria, respectively. The zone of bacterial growth inhibition on Muller Hinton media was measured using the well diffusion method during 24 hours at 37 °C. The results represented as mean ± standard error (SE), and values of $p>0.05$ were determined statistically non-significant, whilst $p<0.05$ and <0.01,0.001, 0.000 were considered substantially different, very significantly different, respectively. The results showed that naked MNPs had antibacterial activity against both examined bacteria, and that the activity increased whenever NPs concentration increased. At 1000 µg/ml, the MNPs demonstrated strong and substantial inhibition zones of 27.5 and 30 mm against S. aureus and E. coli, respectively (Fig. 10).

On the other hand, 1000 µg/ml of GM showed highest growth inhibition zones of 10.8 and 9.5 mm when examined against E. coli and S. aureus, respectively, as presented in Fig. 11. Several studies have been conducted to elucidate the mechanism of iron oxide NPs antibacterial action. One of the mechanisms involved the interaction of opposite charges on the bacterial surface and the potential positive charge of nanoparticle [40]. Due to the extreme existence of a positive charge on the surface of the created MNPs (10.5) in the current investigation, we believe that the attracted electrostatic led to an increase in the contact between the prepared NPs and the tested bacteria. Furthermore, MNPs might be the source of reactive oxygen species (ROS) that limit bacterial growth in the current investigation [41]. Moreover, even at 1000 µg/ml, MNPs with either gelatin or gum Arabic had low antibacterial action against both E. coli and S. aureus. GM had larger inhibition zones of 10.8 and 9.5 mm, while GAM showed 10.8 and 9.3 mm against E. coli and S. aureus, respectively , as shown in Fig. 12.

Cytotoxicity determination of coated and non-coated MNPs

Different concentrations of coated and uncoated MNPs were tested to determine their cytotoxicity against MCF-7 and WRL68, as show in

CC BY

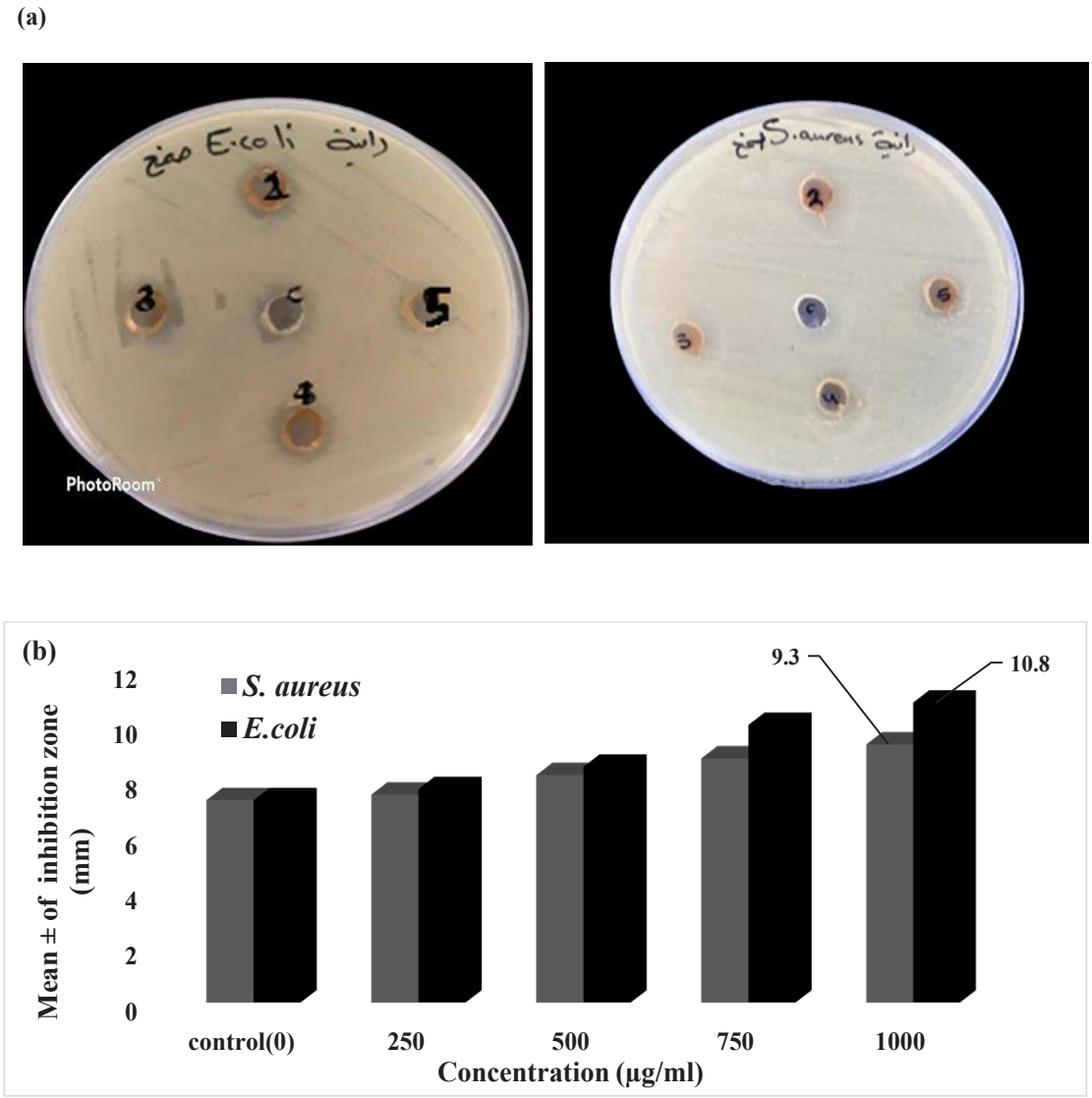

Fig. 12. Growth inhibition zone produced by GAM against bacteria . on Muller-Hinton agar (a) and statistical analyses (b). The control includes only DMSO.

Fig.13. The MTT test was applied to evaluate cell viability after incubating 25, 50, 200, and 400 µg/ml of different manufactured NPs for 24 hours at 37 °C in the presence of 5% CO_2. The significant vitality of MCF-7 was 65.1% when 400 µg/ml of MNPs was used, while it was 75.03% for WRL68. When GAM applied at 400 µg/ml, a substantial viability of MCF-7 and WRL68 were 69.90% and 80.05 %, respectively. Furthermore, when the same concentration was used, the GM exhibit considerable viability of 65.28% and 78.36 %, respectively. Finally, the GAM increased the vitality of both tested cells , while the GM enhanced only the growth of normal cell line.

Treatment of cancer can be either physically with radiation and heat, or chemically using NPs injected into tumor cells to produce reactive oxygen species (ROS) and most critically apoptosis and necrosis in tumor cell populations.

In the presence of 200 µg/mL MNPs, the apoptotic and necrotic populations in MCF-7 cells rose by 61% [29]. Conversely, treating DU145 and PC-3 cell lines for 72 hours with 100 µg/mL MNPs resulted in substantial reduction of cell viability . Moreover, 400 µg/ml of MNPs with a size of 39 nm had substantial antitumor action against kidney

CC BY

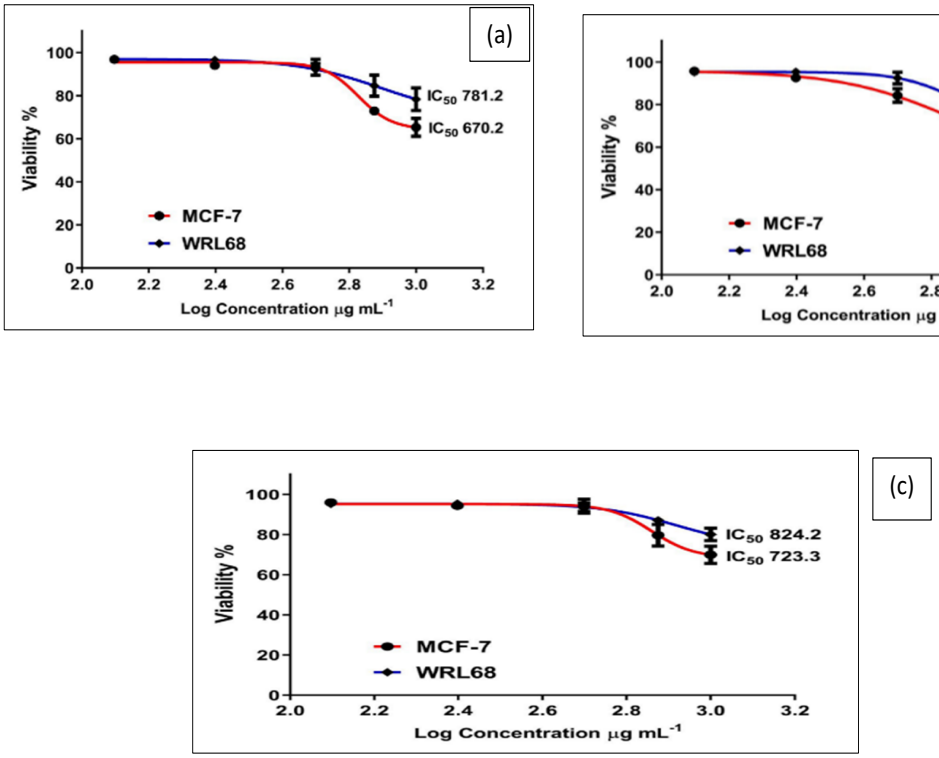

Fig. 13. Cells viability of MCF- 7 and WRL 68 in the presence of MNPs (a), GM (b) and GAM (c).

[30].

CONCLUSIONS

Gelatin and gum Arabic were effectively coated on MNPs produced by the co-precipitated technique. The XRD analysis of the produced nanoparticles confirmed their purity and crystalline character, while FE-SEM images of MNPs GAM and GM have an average particle size not more 55.30 nm. On the other hand, antibacterial activity of MNPs against gram negative and gram-positive bacteria was higher than in coated MNPs. Finally, the MNPs coated with gum Arabic demonstrated low toxicity against MCF-7 and WRL68 cell lines.

ACKNOWLEDGMENTS

The University of Technology in Baghdad, Iraq, has provided funding for this project. The authors appreciate Applied Science's help in preparing and analyzing our samples.

CONFLICT OF INTEREST

The authors declare that there are no conflicts of interest regarding the publication of this manuscript.

REFERENCES

1. Stirling DA. The Nanotechnology Revolution. Jenny Stanford Publishing; 2018.
2. Bhushan B. Introduction to Nanotechnology. Springer Handbook of Nanotechnology: Springer Berlin Heidelberg; 2017. p. 1-19.
3. Hannah W, Thompson PB. Nanotechnology, risk and the environment: a review. Journal of Environmental Monitoring. 2008;10(3):291.
4. Manojlović J. INTRODUCTION TO NANOTECHNOLOGY AND MOLECULAR SELF-ASSEMBLY. Facta Universitatis, Series: Automatic Control and Robotics. 2018;17(2):105.
5. Teja AS, Koh P-Y. Synthesis, properties, and applications of magnetic iron oxide nanoparticles. Progress in Crystal Growth and Characterization of Materials. 2009;55(1-2):22-45.
6. Ahmadi A, Ghanbari D, Nabiyouni G. Facile synthesis of hexagonal strontium ferrite nanostructures and hard magnetic poly carbonate nanocomposite. nano Online: De Gruyter; 2018.
7. Yang Q, Xu Q, Jiang H-L. Metal–organic frameworks meet metal nanoparticles: synergistic effect for enhanced catalysis. Chemical Society Reviews. 2017;46(15):4774-4808.
8. Hedayati K, Kord M, Goodarzi M, Ghanbari D, Gharigh S. Photo-catalyst and magnetic nanocomposites: hydrothermal preparation of core–shell Fe_3O_4@PbS for photo-degradation of toxic dyes. Journal of Materials Science: Materials in Electronics. 2016;28(2):1577-1589.
9. Hedayati K, Azarakhsh S, Saffari J, Ghanbari D. Photo cat-

alyst $CoFe_2O_4$–CdS nanocomposites for degradation of toxic dyes: investigation of coercivity and magnetization. Journal of Materials Science: Materials in Electronics. 2016;27(8):8758-8770.
10. Cartwright A, Jackson K, Morgan C, Anderson A, Britt DW. A Review of Metal and Metal-Oxide Nanoparticle Coating Technologies to Inhibit Agglomeration and Increase Bioactivity for Agricultural Applications. Agronomy. 2020;10(7):1018.
11. Dror Y, Cohen Y, Yerushalmi-Rozen R. Structure of gum arabic in aqueous solution. Journal of Polymer Science Part B: Polymer Physics. 2006;44(22):3265-3271.
12. Alzahrani E. Gum Arabic-Coated Magnetic Nanoparticles For Methylene Blue Removal. International Journal of Innovative Research in Science, Engineering and Technology. 2014;03(08):15118-15129.
13. Young S, Wong M, Tabata Y, Mikos AG. Gelatin as a delivery vehicle for the controlled release of bioactive molecules. Journal of Controlled Release. 2005;109(1-3):256-274.
14. Duconseille A, Astruc T, Quintana N, Meersman F, Sante-Lhoutellier V. Gelatin structure and composition linked to hard capsule dissolution: A review. Food Hydrocolloids. 2015;43:360-376.
15. Illés E, Tombácz E. The effect of humic acid adsorption on pH-dependent surface charging and aggregation of magnetite nanoparticles. Journal of Colloid and Interface Science. 2006;295(1):115-123.
16. Ansari S, Ficiarà E, Ruffinatti F, Stura I, Argenziano M, Abollino O, et al. Magnetic Iron Oxide Nanoparticles: Synthesis, Characterization and Functionalization for Biomedical Applications in the Central Nervous System. Materials. 2019;12(3):465.
17. Sirivat A, Paradee N. Facile synthesis of gelatin-coated Fe_3O_4 nanoparticle: Effect of pH in single-step co-precipitation for cancer drug loading. Materials & Design. 2019;181:107942.
18. Mir AA, Amooey AA, Ghasemi S. Adsorption of direct yellow 12 from aqueous solutions by an iron oxide-gelatin nanoadsorbent; kinetic, isotherm and mechanism analysis. Journal of Cleaner Production. 2018;170:570-580.
19. Saqib S, Munis MFH, Zaman W, Ullah F, Shah SN, Ayaz A, et al. Synthesis, characterization and use of iron oxide nano particles for antibacterial activity. Microscopy Research and Technique. 2018;82(4):415-420.
20. Sato T, Kamaguchi A, Nakazawa F. Purification and characterization of hemolysin from Prevotella oris. Journal of Oral Biosciences. 2012;54(2):113-118.
21. Freshney RI. Culture of Animal Cells. John Wiley & Sons, Inc.; 2010.
22. Bao S, Li K, Ning P, Peng J, Jin X, Tang L. Highly effective removal of mercury and lead ions from wastewater by mercaptoamine-functionalised silica-coated magnetic nano-adsorbents: Behaviours and mechanisms. Applied Surface Science. 2017;393:457-466.
23. Budiredla N, Kumar A, Thota S, Kumar J. Synthesis and Optical Characterization of $Mg_{1-x}Ni_xO$ Nanostructures. ISRN Nanomaterials. 2012;2012:1-8.
24. Gaihre B, Hee Lee Y, Seob Khil M, Keun Yi H, Yong Kim H. In-vitro cytotoxicity and cell uptake study of gelatin-coated magnetic iron oxide nanoparticles. Journal of Microencapsulation. 2011;28(4):240-247.
25. Zamani H, Rastegari B, Varamini M. Antioxidant and anti-cancer activity of Dunaliella salina extract and oral drug delivery potential via nano-based formulations of gum Arabic coated magnetite nanoparticles. Journal of Drug Delivery Science and Technology. 2019;54:101278.
26. Jaisingh SJ, Selvam V, Suresh Chandra Kumar M, Thyagarajan K. Studies on Mechanical Properties of Kevlar Fiber Reinforced Iron (III) Oxide Nanoparticles Filled Up/Epoxy Nanocomposites. Advanced Materials Research. 2013;747:409-412.
27. Basavegowda N, Somai Magar KB, Mishra K, Lee YR. Green fabrication of ferromagnetic Fe_3O_4 nanoparticles and their novel catalytic applications for the synthesis of biologically interesting benzoxazinone and benzthioxazinone derivatives. New J Chem. 2014;38(11):5415-5420.
28. Yew YP, Shameli K, Miyake M, Kuwano N, Bt Ahmad Khairudin NB, Bt Mohamad SE, et al. Green Synthesis of Magnetite (Fe_3O_4) Nanoparticles Using Seaweed (Kappaphycus alvarezii) Extract. Nanoscale Res Lett. 2016;11(1):276-276.
29. Dhenadhayalan N, Mythily R, Kumaran R. Fluorescence spectral studies of Gum Arabic: Multi-emission of Gum Arabic in aqueous solution. Journal of Luminescence. 2014;155:322-329.
30. Tharani K, Jegatha Christy A, Sagadevan S, Nehru LC. Photocatalytic and antibacterial performance of iron oxide nanoparticles formed by the combustion method. Chemical Physics Letters. 2021;771:138524.
31. Sun H, Jiao X, Han Y, Jiang Z, Chen D. Synthesis of Fe_3O_4-Au Nanocomposites with Enhanced Peroxidase-Like Activity. European Journal of Inorganic Chemistry. 2012;2013(1):109-114.
32. Banerjee SS, Chen D-H. Fast removal of copper ions by gum arabic modified magnetic nano-adsorbent. Journal of Hazardous Materials. 2007;147(3):792-799.
33. Gaihre B, Khil M, Lee D, Kim H. Gelatin-coated magnetic iron oxide nanoparticles as carrier system: Drug loading and in vitro drug release study. International Journal of Pharmaceutics. 2009;365(1-2):180-189.
34. Clogston JD, Patri AK. Zeta Potential Measurement. Methods in Molecular Biology: Humana Press; 2010. p. 63-70.
35. Zhang L, Yu F, Cole AJ, Chertok B, David AE, Wang J, et al. Gum arabic-coated magnetic nanoparticles for potential application in simultaneous magnetic targeting and tumor imaging. AAPS J. 2009;11(4):693-699.
36. Horst MF, Coral DF, Fernández van Raap MB, Alvarez M, Lassalle V. Hybrid nanomaterials based on gum Arabic and magnetite for hyperthermia treatments. Materials Science and Engineering: C. 2017;74:443-450.
37. Malhotra N, Lee J-S, Liman RAD, Ruallo JMS, Villaflores OB, Ger T-R, et al. Potential Toxicity of Iron Oxide Magnetic Nanoparticles: A Review. Molecules. 2020;25(14):3159.
38. Thakur S, Govender PP, Mamo MA, Tamulevicius S, Thakur VK. Recent progress in gelatin hydrogel nanocomposites for water purification and beyond. Vacuum. 2017;146:396-408.
39. Arakha M, Pal S, Samantarrai D, Panigrahi TK, Mallick BC, Pramanik K, et al. Antimicrobial activity of iron oxide nanoparticle upon modulation of nanoparticle-bacteria interface. Sci Rep. 2015;5:14813-14813.
40. Sidkey N. BIOSYNTHESIS, CHARACTERIZATION AND ANTIMICROBIAL ACTIVITY OF IRON OXIDE NANOPARTICLES SYNTHESIZED BY FUNGI. Al-Azhar Journal of Pharmaceutical

CC BY